Letter

Structured volume-law entanglement in an interacting, monitored Majorana spin liquid

Guo-Yi Zhu,[1,2,*] Nathanan Tantivasadakarn,[3] and Simon Trebst[1]

[1]*Institute for Theoretical Physics, University of Cologne, Zülpicher Straße 77, 50937 Cologne, Germany*

[2]*The Hong Kong University of Science and Technology (Guangzhou), Nansha, Guangzhou 511400, Guangdong, China*

[3]*Walter Burke Institute for Theoretical Physics and Department of Physics, California Institute of Technology, Pasadena, California 91125, USA*

(Received 18 April 2023; accepted 25 October 2024; published 13 December 2024)

Monitored quantum circuits allow for unprecedented dynamical control of many-body entanglement. Here we show that random, measurement-only circuits, implementing the competition of bond and plaquette couplings of the Kitaev honeycomb model, give rise to a structured volume-law entangled phase with subleading $L \ln L$ liquid scaling behavior. This interacting Majorana liquid takes up a highly symmetric, spherical parameter space within the entanglement phase diagram obtained when varying the relative coupling probabilities. The sphere itself is a critical boundary with quantum Lifshitz scaling separating the volume-law phase from proximate area-law phases, a color code or a toric code. An exception is a set of tricritical, self-dual points exhibiting effective (1+1)d conformal scaling at which the volume-law phase and both area-law phases meet. From a quantum information perspective, our results define error thresholds for the color code in the presence of projective error and stochastic syndrome measurements.

DOI: 10.1103/PhysRevResearch.6.L042063

With the advent of digital quantum computing platforms, quantum researchers can now do pioneering work in shaping entanglement in quantum many-body systems at will through the implementation of quantum circuits. In addition to conventional unitary gates, a decisive element turns out to be the inclusion of nonunitary measurements that have been realized to provide an alternative route to the creation of long-range entanglement, either in combination with unitaries [1–19] or even in measurement-only circuits [20–33], without any unitary gate evolution. Instead it is the noncommutativity of the measurement operators that induces entanglement, which can even exhibit volume-law scaling.

In this manuscript we provide an explicit example of random, measurement-only quantum circuits that induce *structured* volume-law phases in two-dimensional (2D) qubit arrays where in addition to an extensive scaling form there is an $L \ln L$ scaling, reminiscent of the conformal scaling of quantum liquids with a nodal Fermi surface [36,37]. Our model circuit, schematically illustrated in Fig. 1(a), randomly samples the bond and plaquette couplings of the Kitaev honeycomb model, which can be either represented as two- or six-qubit Clifford gates or, alternatively, thought of as Majorana bilinears and a six-Majorana interaction term. Crucially, the two types of couplings are not only noncommuting but also stabilize different topological states of matter—a toric code stabilized by the bilinear interactions [38] versus a color code induced by the plaquette interaction [39,40]. Some of this competition has been previously explored [34,35] concentrating on the bilinear couplings only, i.e., a monitored circuit analog of the Kitaev honeycomb model [38]. There it was shown that the frustration of the noncommuting bilinear couplings induce a gapless spin liquid with $L \ln L$ Fermi-surface-like entanglement entropy [34,35], contrasting the Majorana Dirac cones of the Kitaev spin liquid. The time-reversal symmetry breaking was later discussed in Ref. [41] with a map to the nonorientable statistical loop model in space-time. Here, we depart the free Majorana fermion scenario by including the additional plaquette coupling and show that this has a dramatic effect on the entanglement structure of the many-qubit system. The entanglement phase diagram, illustrated using barycentric coordinates of the probabilities of the four competing terms, is dominated by the emergence of an *interacting* Majorana liquid. Inside a spherically bounded phase towards the center of the tetrahedron [Fig. 1(b)] we find volume-law scaling of the entanglement entropy with an additional $L \ln L$ contribution, inherited from the noninteracting Majorana liquid phase [34,35] inside the circular cut of this sphere with the (noninteracting) base plane of our tetrahedron (marked in yellow in the phase diagram). Such a state withstands a structureless thermalized state [42,43] but rather implies the existence of an extensive number of conserved gapless modes like in a Fermi liquid [44,45]. We therefore identify this phase with an *interacting Majorana liquid*, akin to an interacting Landau-Fermi liquid versus a free-fermion metallic state.

The phase boundary of this interacting Majorana liquid, numerically determined in Fig. 2, approximates a perfect sphere tangent to the edges of the tetrahedron. On this

*Contact author: guoyizhu@hkust-gz.edu.cn

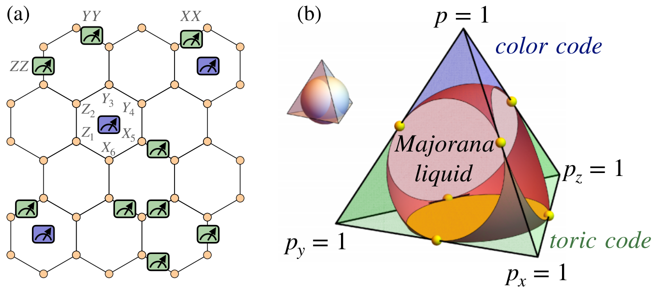

FIG. 1. Schematics of model and phase diagram. (a) (2+1)d random measurement-only circuit on the honeycomb lattice with physical qubits on the sites. Measurements are performed over randomly chosen local bond or plaquette operators, as schematically shown. (b) Schematic quaternary phase diagram drawn as a tetrahedron. A sphere tangent to the edges of the tetrahedron cuts the tetrahedron (inset) into four gapped phases separated by a bulk gapless phase. The top corner of the tetrahedron stands for the topological color code, while the three bottom corners correspond to the toric code. The bottom plane of the tetrahedron corresponds to the monitored Kitaev honeycomb model [34,35], i.e., a free-fermion limit. Entanglement structure: The gapless bulk phase enclosed by the sphere is an *interacting Majorana liquid* with coexisting volume-law and $L \ln L$ entanglement scaling. At its boundary (red sphere) it exhibits quantum Lifshitz scaling. The yellow disk at the bottom as well as the yellow (self-dual) dots at the edge centers indicate $L \ln L$ scaling entanglement beyond a pure area-law.

spherical boundary we find quantum Lifshitz scaling of the entanglement entropy. At the six tangent points we find a dimensional reduction into stacked (1+1)d percolation models and a rigorous duality that can flip each edge of the tetrahedron, and thus the six edge centers are self-dual critical points. Upon perturbation along the edges, they immediately flow to the gapped corner phases of the tetrahedron, while perturbation perpendicular to the edges flow them into the volume-law gapless liquid. The six solvable edges with their self-dual points pin the global topology of the phase diagram. Nevertheless, the almost perfect spherical geometry of the phase boundary indicates an additional hidden rotation symmetry.

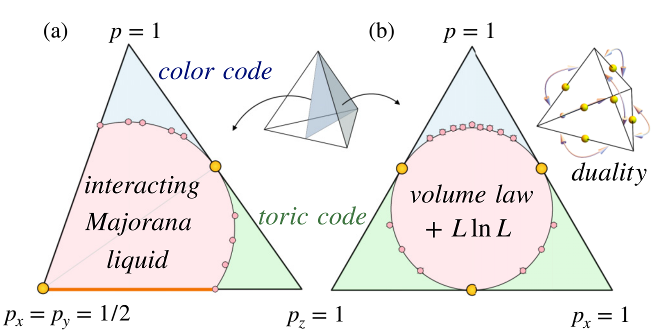

FIG. 2. Cuts through the tetrahedral phase diagram. Panel (a) shows a middle cut plane, described by $p_x = p_y$. (b) The side face of the tetrahedron described by $p_y = 0$. The location of phase transitions (pink dots) have been deduced from the finite-size scaling of the tripartite entanglement [see, e.g., Fig. 4(a) below] by sweeping p and p_z. The solid line is a sphere tangent to the edge of the tetrahedron. The yellow dots indicate self-dual points at the edge centers of the tetrahedron, with the inset on the right illustrating the dualities. The bottom orange line indicates the noninteracting Majorana liquid.

Model. We consider a random, measurement-only circuit on a honeycomb lattice of size $N = 2L^2$, see Fig. 1(a). In each microstep we measure a single, randomly chosen Kitaev-type bond-dependent interaction $K = Z_A Z_B$, $(X_A X_B)$, $(Y_A Y_B)$ with probability $p_{x(y)(z)}$, or alternatively, measure the six-spin interaction $V = Z_1 Z_2 X_3 X_4 Y_5 Y_6$ with probability p. One sweep (which we denote as one time unit) consists of L^2 such random measurements. The noncommuting nature of the measured operators (also within a sweep) is the crucial ingredient to frustration physics and dynamics [22,34,35]. Note that V is distinct from the conserved Wilson plaquette operator $W = X_1 Y_2 Z_3 X_4 Y_5 Z_6$ and does *not* commute with all the bond checks. In a rotated qubit representation, W and V together stabilize a topological color code [39]. In the fermion representation [38], where each spin is factorized into a Majorana fermion c_j and a gauge field $u_l = \pm 1$, $K = iu c_A c_B$ is the Majorana fermion hopping, $W = \prod_{l \in \hexagon} u_l$ stabilizes the gauge flux, while $V = -iu_{12} u_{34} u_{56} (c_1 c_2 c_3 c_4 c_5 c_6)$ is the gauged six-Majorana stabilizer of the Majorana surface code [40].

In executing our circuit, we start from an initial flux-free state $|\psi\rangle = (\prod_q \frac{1+W_q}{2}) |\uparrow\rangle^{\otimes N}$ [46]. This initial state we evolve until it reaches its steady state, i.e., for sufficiently long times of order $O(L)$. Since the gauge flux is frozen in our circuit model, the ensuing dynamics is solely carried by the Majorana fermions subject to a competition of hopping and plaquette interactions. Our model is thus a Clifford stabilizer circuit [47] analog to the ground state of an interacting Majorana Hamiltonian $H \sim (1-p)K + pV$, interpolating between the Kitaev honeycomb model and the Majorana surface code model [40]. While this interacting (2+1)d lattice Hamiltonian is in general hard to solve, the Clifford stabilizer circuit allows for efficient numerical calculation with polynomial scaling by keeping track of the N generators of the stabilizer group rather than the 2^N-dimensional quantum many-body wave function.

Entanglement phase diagram. The key feature characterizing the dynamically generated, steady-state phases of our monitored quantum circuit is the von Neumann entanglement entropy. To set the stage, let us first consider the noninteracting setup corresponding to the bottom plane of our tetrahedron. Here the random bond checks measure the local Majorana fermion parity and effectively teleport single Majorana fermions [48]. The final state is a Gaussian fermionic state, a product of long-range Majorana pairs, that exhibits $L \ln L$ Fermi-surface-like entanglement entropy [34,35] (see also the Supplemental Material [49]). By viewing each Majorana pair as a dimer and upon disorder average that crucially restores translation symmetry, one can view this noninteracting Majorana liquid as a dynamically generated density matrix analog of the long-range resonating-valence-bond (RVB) state [50]. If we depart the free-fermion setting, an onset of six-Majorana interaction measurements glues the Majorana pairs beyond the Gaussian fermion state. A priori, it is not clear whether the paired free Majoranas and their consequent $L \ln L$ entanglement can survive this interaction effect.

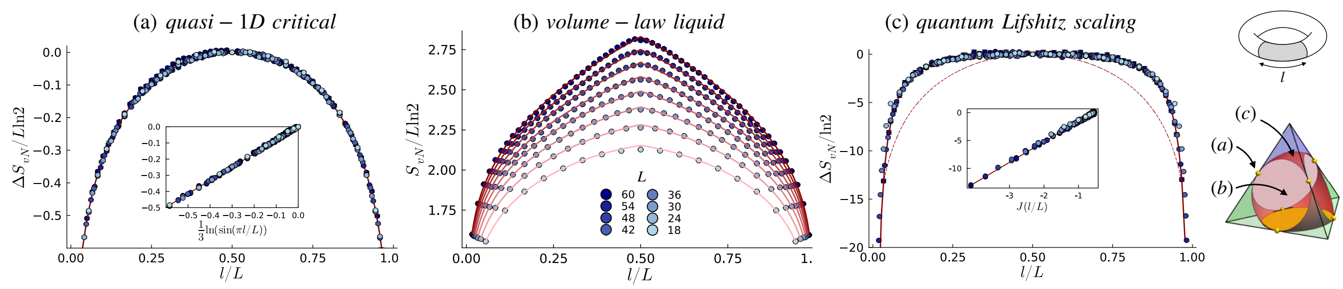

FIG. 3. Entanglement structure of three forms of gapless matter characterized by their entanglement entropy scaling. (a) Self-dual point $p = p_z = 1/2$, $p_x = p_y = 0$ with dimensional reduction. We subtract the area-law background to exhibit data collapse for the universal super-area-law correction $\Delta S_{vN} \equiv [S_{vN}(l) - S_{vN}(L/2)]/L = \frac{c}{3}\ln\sin\frac{\pi l}{L}$. We fit $c = 0.829(2)\ln 2$. (b) Interacting Majorana liquid with weak volume-law scaling plus strong $L\ln L$ correction, at the centroid of the tetrahedron $p_x = p_y = p_z = 1/4$. The red lines illustrate the fitting scaling function, for $a = 1.615(4)\ln 2$, $v = 0.00951(7)\ln 2$, $c = 0.642(7)\ln 2$, $c' = 2.2(2)\ln 2$, $\gamma = 1.4(1)\ln 2$. See SM for a view of each decomposed fractions. (c) Entanglement entropy at the critical point between interacting Majorana liquid and Majorana surface code $p_c = 0.683$, $p_x = p_y = p_z$. The solid red line denotes the scaling function with best-fit coefficients $\beta = 3.67(3)\ln 2$, $\lambda = 3.8(2)\ln 2$. The dashed line shows the best fit of scaling function $\ln\sin(\pi l/L)$ for comparison. The insets show data collapses for rescaled horizontal axes.

To explore this, we analyze the von Neumann entanglement entropy [51] for a bipartition of the torus (of length L-by-L) into two cylinders with smooth boundary of fixed length L but varying subsystem bulk length l, see the inset of Fig. 3. We consider a most general scaling ansatz of the form

$$S_{vN}(l, L) = v \cdot \mathrm{vol}(l, L) + \frac{cL + c'}{3}\ln\left(\frac{L}{\pi}\sin\frac{\pi l}{L}\right) + aL - \gamma. \tag{1}$$

Here $\mathrm{vol}(l, L) = 2Ll\ln 2 - 2^{4Ll-N-1}$ ($l \leqslant L/2$) is the volume-law contribution with a leading-order Page correction [53], the second term is a subleading contribution [54,55] that can account for gapless modes akin to a Fermi surface (when viewed as slices of (1+1)d conformal field theories (CFTs) [44,56]). The $O(1)$ correction γ is known as the topological entanglement entropy (TEE) [57,58]. The prefactors v, c, a are nonuniversal and fitted in our numerics, though c is reminiscent of the central charge in a (1+1)d CFT.

Let us first consider the case $p = p_z = 1/2$, $p_x = p_y = 0$, which is one of the exactly solvable, self-dual points. Coming from the Majorana surface code, the six-Majorana plaquette interactions stabilize anyon excitations on the plaquettes, while the ZZ-bond Majorana bilinear fluctuates these anyons *only* along the z direction [40]. Thus the model is effectively decoupled into stacks of anyon chains and a duality can swap the plaquette interaction and the Majorana bilinear, akin to the Kramers-Wannier duality of the quantum Ising chain [59]. For further discussion, see the underlying frustration graph given in the SM [60]. Each chain can be mapped to a classical 2D bond percolation problem [62,63], where the prefactor c is exactly calculated employing CFT to be $c = 3\sqrt{3}\ln 2/(2\pi)$, perfectly consistent with our numerical results in Fig. 3(a).

Except the self-dual points, the effect of a nonvanishing Majorana interaction is the immediate formation of a volume-law contribution. As an example we show, in Fig. 3(b), the entanglement entropy for the centroid of the tetrahedral phase diagram, $p_{x(y)(z)} = p = 1/4$. The growth of the entanglement entropy with increasing l clearly goes beyond the arclike $\ln(\sin\frac{\pi l}{L})$ scaling of the free-fermion limit, but instead an almost linear increase is found for lengths $l \sim L/2$, resulting in a cusplike feature known from Page scaling [53]. Note that even though a volume law is the leading contribution in the $L \to \infty$ (thermodynamic) limit, its prefactor turns out to be *two orders of magnitude smaller* than the coefficient of the subleading $L\ln L$ correction, which for small system sizes quantitatively dominates. The existence of such an $L\ln L$ correction implies that the volume-law phase is not structureless, which we further comment on in the Discussion section below. When one moves along the bond-isotropic line $p_{x(y)(z)} = (1-p)/3$ and increases p from 0, the volume-law prefactor rapidly but smoothly grows to a peak value around $p \sim 0.15$ before decreasing again and fading away around $p \sim 0.5$, as shown explicitly in the SM. To diagnose the precise critical point of the transition out of the volume-law phase, we resort to the tripartite mutual information [64].

At these interacting critical points, the entanglement entropy is found to significantly deviate from the $L\ln L$ correction [65] in Eq. (1) and instead exhibits quantum Lifshitz scaling [66,67], originally derived for the gapless dimer RVB state (quantum Lifshitz field theory [68]),

$$S_{vN} = aL + \beta J(l/L) + \cdots,$$

where $J(x) = -\ln\frac{\theta_3(i\lambda x)\theta_3[i\lambda(1-x)]}{\eta(2ix)\eta[2i(1-x)]}$, with θ_3 the Jacobi-θ function and η the Dedekind-η function [66,67,69]. An example of such quantum Lifshitz scaling is shown in Fig. 3(c). On a speculative note, this Lifshitz scaling might be a harbinger of space-time anisotropy with a dynamical critical exponent $z = 2$ (though counterexamples [67] indicate that no such stringent connection can be made), which would possibly allow us to connect this scaling form to the Lifshitz transition of Fermi surface topologies [70]—an appealing completion to our scenario of a sequence of transitions from noninteracting to interacting to vanishing Fermi liquid as one ascends the vertical direction in our tetrahedral phase diagram.

Topological codes and phase transitions. Let us round off our discussion of the entanglement phase diagram by looking at the four corner phases, which are gapped area-law phases realizing either a toric code (for the three bottom corners) or a color code (near the top of our tetrahedron). Starting from one of these gapped phases, we can discuss the entanglement

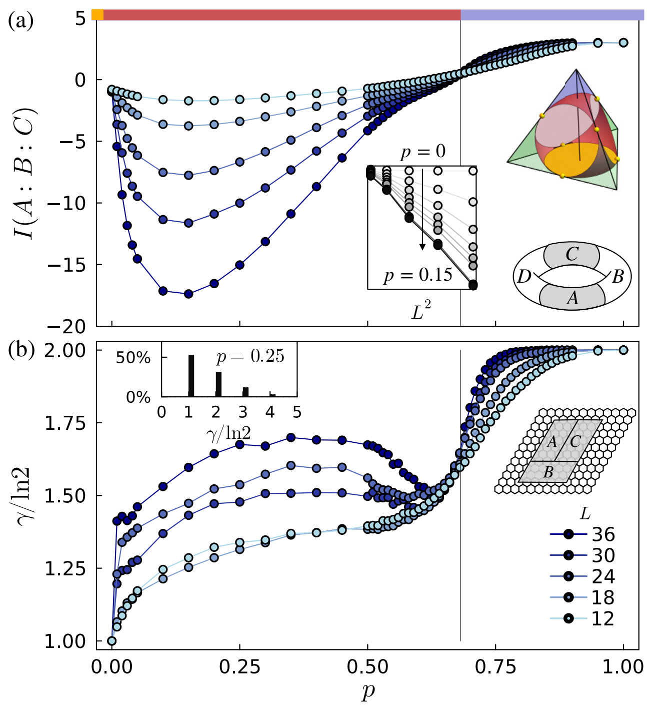

FIG. 4. Topological and entanglement phase transition along the bond-isotropic line $p_{x(y)(z)} = (1-p)/3$. (a) Tripartite mutual information (TMI) between three cylinders (see inset). Finite-size scaling gives $p_c = 0.682(4)$, very close to the exact boundary of the sphere $p_c = (1+\sqrt{3})/4 = 0.683\,01\ldots$, and $1/\nu = 1.01(6)$. For the phase region between $p \in (0, p_c)$, the TMI diverges $I \propto -L^2$ with system size, as shown in the inset for the window $p \leqslant 0.15$. (b) Topological entanglement entropy. Inset shows the distribution of γ among the disorder ensemble for $p = 0.25$. Data is averaged over 10 000 disorder realizations for $L < 30$ and 5000 samples for $L \geqslant 30$.

transition into the interacting Majorana liquid. Mapping out the phase boundary can be done, as before, by computing the tripartite mutual information (TMI),

$$I(A:B:C) = S_A + S_B + S_C - S_{AB} - S_{BC} - S_{AC} + S_{ABC},$$

for a partition of the torus into four cylinders [inset of Fig. 4(a)]. As shown in Fig. 4(a), away from the free-fermion limit $p = 0$ where $I = -1$ [34,35], the TMI is *extensive* for the interacting liquid phase, i.e., $I(A:B:C) \propto -L^2$, as shown in the inset. Such an indicator of information scrambling [71] is consistent with the volume-law entanglement entropy we found earlier. In the color code limit $p \to 1$, $I(A:B:C) = +3$ due to three independent effective Bell pairs between A and C, formed by the product of plaquettes of the color code (its plaquettes being three colorable when $L \mod 3 = 0$). In between, the crossing point indicates an entanglement phase transition from the interacting Majorana liquid to the Majorana surface code, which we used to quantitatively map out the phase diagram of Fig. 2.

From a quantum information perspective, we can interpret the area- to volume-law transition out of the color code as an *error threshold* for the color code subject to projective bond errors and stochastic syndrome measurements. This is best revealed in the TEE [57,58], calculated for the tripartite geometry in the inset of Fig. 4(b). In the color code phase, it shows a plateau at $2\ln 2$, reflecting the two bits of information contributed from the gauge *and* Majorana sector (versus one bit in the toric code where only the gauge sector contributes). At the threshold p_c of the color code, the TEE drops from its plateau value, signaling the breakdown of topological order. This transition gives a fundamental upper bound of the decoding threshold for the color code under such noise. The TEE is nonquantized in the interacting liquid regime (while still showing a system size dependence, growing with increasing L). We note that the volume-law phase can still be used as a code space with quantum error correction [72,73], but (in light of the small volume-law prefactor) it might be much less effective in storing logical quantum information; see SM [49] for purification dynamics indicating a corruption of the code space.

Outlook. Our highly symmetric phase diagram calls for an analytical understanding. One step in this direction is to pursue a coupled-wire approach: Start from a bottom edge, which corresponds to stacked monitored Majorana chains, and turn on either the Majorana hopping or Majorana interactions. The former coupling leads to the free-fermion liquid within the bottom plane, while the latter sets off a flow to the volume-law liquid in the side plane of the tetrahedron. Despite this distinction, both directions show surprisingly similar geometrical phase boundaries: a circle, see Fig. 2. This might be related to the similarity of their frustration graph structure, which can both be viewed as a stack of bipartite horizontal chains, with interchain degree-4 nodes relating the two sublattices (see SM [49]). We note that our circuit model can alternatively be implemented by a unitary circuit with two-qubit gates and single-qubit measurements only (see SM [49]).

Discussion. A hallmark of equilibrium quantum states of matter is their boundary-law entanglement scaling [74], which for Fermi liquids experiences a mild violation in an $L\ln L$ "super-area-law" contribution [36,37,44,45]. In contrast, the nonequilibrium Fermi liquid discussed in our work exhibits an extensive (volume-law scaling) entanglement entropy, with a subleading $L\ln L$ contribution in (2+1) dimensions. The existence of this subleading term not only distinguishes our state from a *thermal* steady state, but it might prove to be essential: In its (1+1)d analogs, the subleading $\ln L$ correction indicates a *protection mechanism* of the volume-law entanglement structure as it originates from a power-law distribution of stabilizers [75] that counteract the detrimental effects of local projective measurements on long-range stabilizers. One might argue that a similar mechanism plays out in (2+1)d quantum liquids, indicating an essential role for the $L\ln L$ term to allow for a *stable* volume-law phase [76].

The coexistence of volume-law and $L\ln L$ scaling we report here might bear some resemblance with the observation of *quantum many-body scars* [77,78] in (1+1)d models. There one observes a *weak ergodicity breaking* that manifests itself in a tower of $\ln L$ entangled nonthermal eigenstates [79] coexisting with the otherwise volume-law entangled thermal states [42,43]. Instead of starting from an ergodic phase, our model arrives at a similar entanglement structure, in a (2+1)d generalization, from a proximate (super) area-law phase, i.e., it exhibits *weak information scrambling*.

A characteristic of our model is its *randomness*, manifest in the space-time disorder of the circuit, in addition to measurement outcomes, which results in an *ensemble of disordered pure states*. This randomness spoils translation symmetries for each individual disorder realization (of the circuit), which makes it possible to have a stable Majorana Fermi surface, even in the presence of time-reversal symmetry [80–82]. The disorder average restores the symmetries on a statistical level. The disorder-averaged entanglement represents *typical pure wave functions* in the ensemble, but *not* the average density matrix, which may be also interpreted as a translationally invariant state in the double Hilbert space [83]. An interesting future direction is to further explore the essential role of randomness, e.g., by imposing space or time translation symmetry into the protocol [84], such as a spatially random Floquet circuit [85] or a quasiperiodic protocol [86].

Let us close with a comment on computational complexity. Nontrivial entanglement structures can arise from the competition of local interactions—either in the steady state of the long-time evolution of a random measurement circuit, as discussed in this manuscript, or in the quantum ground state of a quantum many-body system cooled down under Hamiltonian dynamics. Despite their similar ingredients, the two approaches come with very different simulation costs on a classical computer—an interacting ground state with a Fermi surface is known to create a sign problem [87] in quantum Monte Carlo simulations [88], while we have shown that a similarly entangled state can be simulated with Clifford stabilizer circuits in polynomial time [89]. This leaves us in the fascinating situation that going to the Clifford circuit analog state has *reduced* the computational complexity of simulating an interacting Fermi liquid, a route that should be further explored, for other quantum states of interest, in the future.

Acknowledgments. We thank Michael Buchhold and Xhek Turkeshi for insightful discussions. The Cologne group was partially funded by the Deutsche Forschungsgemeinschaft under Germany's Excellence Strategy–Cluster of Excellence Matter and Light for Quantum Computing (ML4Q) EXC 2004/1–390534769 and within the CRC network TR 183 (Project Grant No. 277101999) as part of Project No. A04 and No. B01. N.T. is supported by the Walter Burke Institute for Theoretical Physics at Caltech. The numerical simulations were performed on the JUWELS cluster at the Forschungszentrum Juelich. G.Y.Z. would like to acknowledge the startup fund in HKUST(GZ).

[1] H. J. Briegel and R. Raussendorf, Persistent entanglement in arrays of interacting particles, Phys. Rev. Lett. **86**, 910 (2001).

[2] R. Raussendorf, S. Bravyi, and J. Harrington, Long-range quantum entanglement in noisy cluster states, Phys. Rev. A **71**, 062313 (2005).

[3] R. Raussendorf, J. Harrington, and K. Goyal, A fault-tolerant one-way quantum computer, Ann. Phys. **321**, 2242 (2006).

[4] A. Bolt, G. Duclos-Cianci, D. Poulin, and T. M. Stace, Foliated quantum error-correcting codes, Phys. Rev. Lett. **117**, 070501 (2016).

[5] L. Piroli, G. Styliaris, and J. I. Cirac, Quantum circuits assisted by local operations and classical communication: Transformations and phases of matter, Phys. Rev. Lett. **127**, 220503 (2021).

[6] R. Verresen, N. Tantivasadakarn, and A. Vishwanath, Efficiently preparing Schrödinger's cat, fractons and non-Abelian topological order in quantum devices, arXiv:2112.03061.

[7] N. Tantivasadakarn, R. Thorngren, A. Vishwanath, and R. Verresen, Long-range entanglement from measuring symmetry-protected topological phases, Phys. Rev. X **14**, 021040 (2024).

[8] M. Fisher, V. Khemani, A. Nahum, and S. Vijay, Random quantum circuits, Annu. Rev. Condens. Matter Phys. **14**, 335 (2023).

[9] Y. Li, X. Chen, and M. P. A. Fisher, Quantum Zeno effect and the many-body entanglement transition, Phys. Rev. B **98**, 205136 (2018).

[10] B. Skinner, J. Ruhman, and A. Nahum, Measurement-induced phase transitions in the dynamics of entanglement, Phys. Rev. X **9**, 031009 (2019).

[11] P. Sierant, M. Schirò, M. Lewenstein, and X. Turkeshi, Measurement-induced phase transitions in $(d+1)$-dimensional stabilizer circuits, Phys. Rev. B **106**, 214316 (2022).

[12] T.-C. Lu, L. A. Lessa, I. H. Kim, and T. H. Hsieh, Measurement as a shortcut to long-range entangled quantum matter, PRX Quantum **3**, 040337 (2022).

[13] S. Bravyi, I. Kim, A. Kliesch, and R. Koenig, Adaptive constant-depth circuits for manipulating non-Abelian anyons, arXiv:2205.01933.

[14] G.-Y. Zhu, N. Tantivasadakarn, A. Vishwanath, S. Trebst, and R. Verresen, Nishimori's cat: Stable long-range entanglement from finite-depth unitaries and weak measurements, Phys. Rev. Lett. **131**, 200201 (2023).

[15] J. Y. Lee, W. Ji, Z. Bi, and M. P. A. Fisher, Decoding measurement-prepared quantum phases and transitions: From Ising model to gauge theory, and beyond, arXiv:2208.11699.

[16] A. J. Friedman, C. Yin, Y. Hong, and A. Lucas, Locality and error correction in quantum dynamics with measurement, arXiv:2206.09929.

[17] N. Tantivasadakarn, R. Verresen, and A. Vishwanath, Shortest route to non-Abelian topological order on a quantum processor, Phys. Rev. Lett. **131**, 060405 (2023).

[18] N. Tantivasadakarn, A. Vishwanath, and R. Verresen, Hierarchy of topological order from finite-depth unitaries, measurement and feedforward, PRX Quantum **4**, 020339 (2023).

[19] M. Iqbal, N. Tantivasadakarn, T. M. Gatterman, J. A. Gerber, K. Gilmore, D. Gresh, A. Hankin, N. Hewitt, C. V. Horst, M. Matheny, T. Mengle, B. Neyenhuis, A. Vishwanath, M. Foss-Feig, R. Verresen, and H. Dreyer, Topological order from measurements and feed-forward on a trapped ion quantum computer, Commun. Phys. **7**, 205 (2024).

[20] A. Lavasani, Y. Alavirad, and M. Barkeshli, Measurement-induced topological entanglement transitions in symmetric random quantum circuits, Nat. Phys. **17**, 342 (2021).

[21] S. Sang and T. H. Hsieh, Measurement-protected quantum phases, Phys. Rev. Re. **3**, 023200 (2021).

[22] M. Ippoliti, M. J. Gullans, S. Gopalakrishnan, D. A. Huse, and V. Khemani, Entanglement phase transitions in measurement-only dynamics, Phys. Rev. X **11**, 011030 (2021).

[23] K. Klocke and M. Buchhold, Topological order and entanglement dynamics in the measurement-only XZZX quantum code, Phys. Rev. B **106**, 104307 (2022).

[24] A. Lavasani, Y. Alavirad, and M. Barkeshli, To opological order and criticality in $(2+1)$d monitored random quantum circuits, Phys. Rev. Lett. **127**, 235701 (2021).

[25] M. B. Hastings and J. Haah, Dynamically generated logical qubits, Quantum **5**, 564 (2021).

[26] D. Aasen, Z. Wang, and M. B. Hastings, Adiabatic paths of Hamiltonians, symmetries of topological order, and automorphism codes, Phys. Rev. B **106**, 085122 (2022).

[27] M. Davydova, N. Tantivasadakarn, and S. Balasubramanian, Floquet codes without parent subsystem codes, PRX Quantum **4**, 020341 (2023).

[28] M. S. Kesselring, J. C. M. de la Fuente, F. Thomsen, J. Eisert, S. D. Bartlett, and B. J. Brown, Anyon condensation and the color code, PRX Quantum **5**, 010342 (2024).

[29] H. Bombin, D. Litinski, N. Nickerson, F. Pastawski, and S. Roberts, Unifying flavors of fault tolerance with the ZX calculus, Quantum **8**, 1379 (2024).

[30] Z. Zhang, D. Aasen, and S. Vijay, *X*-cube Floquet code: A dynamical quantum error correcting code with a subextensive number of logical qubits, Phys. Rev. B **108**, 205116 (2023).

[31] D. Vu, A. Lavasani, J. Y. Lee, and M. P. A. Fisher, Measurement-induced Floquet enriched topological order, Phys. Rev. Lett. **132**, 070401 (2024).

[32] J. Y. Lee, Y.-Z. You, and C. Xu, Symmetry protected topological phases under decoherence, arXiv:2210.16323.

[33] J. Y. Lee, C.-M. Jian, and C. Xu, Quantum criticality under decoherence or weak measurement, PRX Quantum **4**, 030317 (2023).

[34] A. Lavasani, Z.-X. Luo, and S. Vijay, Monitored quantum dynamics and the Kitaev spin liquid, Phys. Rev. B **108**, 115135 (2023).

[35] A. Sriram, T. Rakovszky, V. Khemani, and M. Ippoliti, Topology, criticality, and dynamically generated qubits in a stochastic measurement-only Kitaev model, Phys. Rev. B **108**, 094304 (2023).

[36] M. M. Wolf, Violation of the entropic area law for fermions, Phys. Rev. Lett. **96**, 010404 (2006).

[37] D. Gioev and I. Klich, Entanglement entropy of fermions in any dimension and the Widom conjecture, Phys. Rev. Lett. **96**, 100503 (2006).

[38] A. Kitaev, Anyons in an exactly solved model and beyond, Ann. Phys. **321**, 2 (2006).

[39] H. Bombin and M. A. Martin-Delgado, Topological quantum distillation, Phys. Rev. Lett. **97**, 180501 (2006).

[40] S. Vijay, T. H. Hsieh, and L. Fu, Majorana fermion surface code for universal quantum computation, Phys. Rev. X **5**, 041038 (2015).

[41] K. Klocke, D. Simm, G.-Y. Zhu, S. Trebst, and M. Buchhold, Entanglement dynamics in monitored Kitaev circuits: Loop models, symmetry classification, and quantum Lifshitz scaling, arXiv:2409.02171.

[42] J. M. Deutsch, Quantum statistical mechanics in a closed system, Phys. Rev. A **43**, 2046 (1991).

[43] M. Srednicki, Chaos and quantum thermalization, Phys. Rev. E **50**, 888 (1994).

[44] B. Swingle, Conformal field theory approach to Fermi liquids and other highly entangled states, Phys. Rev. B **86**, 035116 (2012).

[45] W. Ding, A. Seidel, and K. Yang, Entanglement entropy of Fermi liquids via multidimensional bosonization, Phys. Rev. X **2**, 011012 (2012).

[46] Such states can be prepared by projectively measuring W_q over every plaquette q once upon the spin product state $|\uparrow\rangle^{\otimes N}$ in a finite depth circuit. $|\uparrow\rangle$ is the eigenstate of Pauli Z. Note that static flux defects with $W_q = -1$ would result in exactly the same entanglement properties.

[47] S. Aaronson and D. Gottesman, Improved simulation of stabilizer circuits, Phys. Rev. A **70**, 052328 (2004).

[48] P. Bonderson, M. Freedman, and C. Nayak, Measurement-only topological quantum computation, Phys. Rev. Lett. **101**, 010501 (2008).

[49] See Supplemental Material at http://link.aps.org/supplemental/10.1103/PhysRevResearch.6.L042063 for (i) the frustration graph of the stabilizer dynamics; (ii) an alternative circuit implementation using only single-qubit measurement; (iii) supplementary data of free Majorana and structured volume law phase; (iv) supplementary data for topological entanglement entropy; (v) purification dynamics.

[50] P. Anderson, Resonating valence bonds: A new kind of insulator? Mater. Res. Bull. **8**, 153 (1973).

[51] The entanglement entropy can be efficiently calculated from the number of linearly independent stabilizers supported in a subsystem subtracted by its number of qubits [47], which can be numerically computed by the rank of the stabilizer matrix over the binary field [52].

[52] C. Fieker, W. Hart, T. Hofmann, and F. Johansson, Nemo/hecke Computer algebra and number theory packages for the julia programming language, in *Proceedings of the 2017 ACM on International Symposium on Symbolic and Algebraic Computation, ISSAC'17* (ACM Press, New York, NY, 2017), pp. 157–164.

[53] D. N. Page, Average entropy of a subsystem, Phys. Rev. Lett. **71**, 1291 (1993).

[54] P. Calabrese and J. Cardy, Entanglement entropy and quantum field theory, J. Stat. Mech. (2004) P06002.

[55] X. Turkeshi, R. Fazio, and M. Dalmonte, Measurement-induced criticality in $(2+1)$-dimensional hybrid quantum circuits, Phys. Rev. B **102**, 014315 (2020).

[56] B. Swingle, Entanglement entropy and the Fermi surface, Phys. Rev. Lett. **105**, 050502 (2010).

[57] A. Kitaev and J. Preskill, Topological entanglement entropy, Phys. Rev. Lett. **96**, 110404 (2006).

[58] M. Levin and X.-G. Wen, Detecting Topological order in a ground state wave function, Phys. Rev. Lett. **96**, 110405 (2006).

[59] J. B. Kogut, An introduction to lattice gauge theory and spin systems, Rev. Mod. Phys. **51**, 659 (1979).

[60] Note that the edge can also be alternatively mapped to a Wen plaquette model [61] (i.e., a basis-rotated version of the toric code) subjected to uniform Z-type measurements.

[61] X.-G. Wen, Quantum orders in an exact soluble model, Phys. Rev. Lett. **90**, 016803 (2003).

[62] N. Lang and H. P. Büchler, Entanglement transition in the projective transverse field Ising model, Phys. Rev. B **102**, 094204 (2020).

[63] A. Nahum and B. Skinner, Entanglement and dynamics of diffusion-annihilation processes with Majorana defects, Phys. Rev. Res. **2**, 023288 (2020).

[64] A. Zabalo, M. J. Gullans, J. H. Wilson, S. Gopalakrishnan, D. A. Huse, and J. H. Pixley, Critical properties of the measurement-induced transition in random quantum circuits, Phys. Rev. B **101**, 060301(R) (2020).

[65] H. Ju, A. B. Kallin, P. Fendley, M. B. Hastings, and R. G. Melko, Entanglement scaling in two-dimensional gapless systems, Phys. Rev. B **85**, 165121 (2012).

[66] J.-M. Stéphan, H. Ju, P. Fendley, and R. G. Melko, Entanglement in gapless resonating-valence-bond states, New J. Phys. **15**, 015004 (2013).

[67] X. Chen, G. Y. Cho, T. Faulkner, and E. Fradkin, Scaling of entanglement in 2+ 1-dimensional scale-invariant field theories, J. Stat. Mech. (2015) P02010.

[68] E. Ardonne, P. Fendley, and E. Fradkin, Topological order and conformal quantum critical points, Ann. Phys. **310**, 493 (2004).

[69] $J(x)$ is derived by mapping the exact dimer wave function into the 2D free boson CFT and tracing out the boson for its partition function [66]. Note that at the limit $x \ll 1$, the area-law correction $J(x) \sim -\frac{\pi}{24x}$, in contrast to $\ln\sin(x\pi) \sim \ln x$ for the (1+1)d CFT, and their respective prefactors β and c take qualitatively similar meaning as universal characterization of entangled degrees of freedom.

[70] G. E. Volovik, Topological Lifshitz transitions, Low Temp. Phys. **43**, 47 (2017).

[71] P. Hosur, X.-L. Qi, D. A. Roberts, and B. Yoshida, Chaos in quantum channels, J. High Energy Phys. 02 (2016) 004.

[72] S. Choi, Y. Bao, X.-L. Qi, and E. Altman, Quantum error correction in scrambling dynamics and measurement-induced phase transition, Phys. Rev. Lett. **125**, 030505 (2020).

[73] M. J. Gullans and D. A. Huse, Dynamical purification phase transition induced by quantum measurements, Phys. Rev. X **10**, 041020 (2020).

[74] J. Eisert, M. Cramer, and M. B. Plenio, Colloquium: Area laws for the entanglement entropy, Rev. Mod. Phys. **82**, 277 (2010).

[75] Y. Li, X. Chen, and M. P. A. Fisher, Measurement-driven entanglement transition in hybrid quantum circuits, Phys. Rev. B **100**, 134306 (2019).

[76] It remains an interesting question to explore whether this entanglement structure remains stable when moving away from Clifford stabilizer circuits.

[77] M. Serbyn, D. A. Abanin, and Z. Papić, Quantum many-body scars and weak breaking of ergodicity, Nat. Phys. **17**, 675 (2021).

[78] A. Chandran, T. Iadecola, V. Khemani, and R. Moessner, Quantum many-body scars: A quasiparticle perspective, Annu. Rev. Condens. Matter Phys. **14**, 443 (2023).

[79] S. Moudgalya, N. Regnault, and B. A. Bernevig, Entanglement of exact excited states of Affleck-Kennedy-Lieb-Tasaki models: Exact results, many-body scars, and violation of the strong eigenstate thermalization hypothesis, Phys. Rev. B **98**, 235156 (2018).

[80] V. Chua, H. Yao, and G. A. Fiete, Exact chiral spin liquid with stable spin Fermi surface on the kagome lattice, Phys. Rev. B **83**, 180412(R) (2011).

[81] C. R. Laumann, A. W. W. Ludwig, D. A. Huse, and S. Trebst, Disorder-induced Majorana metal in interacting non-Abelian anyon systems, Phys. Rev. B **85**, 161301(R) (2012).

[82] J. Knolle, R. Moessner, and N. B. Perkins, Bond-disordered spin liquid and the honeycomb iridate $H_3LiIr_2O_6$: Abundant low-energy density of states from random Majorana hopping, Phys. Rev. Lett. **122**, 047202 (2019).

[83] Y. Bao, R. Fan, A. Vishwanath, and E. Altman, Mixed-state topological order and the errorfield double formulation of decoherence-induced transitions, arXiv:2301.05687.

[84] G. M. Sommers, D. A. Huse, and M. J. Gullans, Crystalline quantum circuits, PRX Quantum **4**, 030313 (2023).

[85] A. Chan, A. De Luca, and J. T. Chalker, Solution of a minimal model for many-body quantum chaos, Phys. Rev. X **8**, 041019 (2018).

[86] P. T. Dumitrescu, R. Vasseur, and A. C. Potter, Logarithmically slow relaxation in quasiperiodically driven random spin chains, Phys. Rev. Lett. **120**, 070602 (2018).

[87] O. Grossman and E. Berg, Robust Fermi-liquid instabilities in sign problem-free models, Phys. Rev. Lett. **131**, 056501 (2023).

[88] M. Troyer and U.-J. Wiese, Computational complexity and fundamental limitations to fermionic quantum Monte Carlo simulations, Phys. Rev. Lett. **94**, 170201 (2005).

[89] D. Gottesman, The Heisenberg representation of quantum computers, in *Proceedings of the XXII International Colloquium on Group Theoretical Methods in Physics*, edited by S. P. Corney, R. Delbourgo, and P. D. Jarvis (International Press, Cambridge, MA, 1999), pp. 32–43.